









The democratic detrender: Ensemble-Based Removal of the Nuisance Signal in Stellar Time-Series Photometry

DANIEL A. YAHALOMI ^{1,*} DAVID KIPPING ¹ DIANA SOLANO-OROPEZA ^{1,2} MADISON LI ^{3,1} AVISHI PODDAR ¹
XUNHE (ANDREW) ZHANG ¹ YASSINE ABAKIL¹ BEN CASSESE ¹ ALEX TEACHEY ⁴ JIAJING LIU^{5,†}
FARAI SUNDAL^{5,†} AND LILA VALASKOVIC^{5,†}

¹*Department of Astronomy, Columbia University, 550 W 120th St., New York NY 10027, USA*

²*Department of Astronomy, Cornell University, 122 Sciences Drive, Ithaca, NY 14850, USA*

³*Department of Astronomy, Barnard College, 3009 Broadway, New York NY 10027, USA*

⁴*Institute of Astronomy and Astrophysics, Academia Sinica, Taipei 10617, Taiwan*

⁵*Cambridge Rindge and Latin School, Cambridge, MA 02138, USA*

ABSTRACT

Accurate, precise, and computationally efficient removal of unwanted activity that exists as a combination of periodic, quasi-periodic, and non-periodic systematic trends in time-series photometric data is a critical step in exoplanet transit analysis. Throughout the years, many different modeling methods have been used for this process, often called “detrending.” However, there is no community-wide consensus regarding the favored approach. In order to mitigate model dependency, we present an ensemble-based approach to detrending via community-of-models and the **democratic detrender**: a modular and scalable open-source coding package that implements ensemble detrending. The **democratic detrender** allows users to select from a number of packaged detrending methods (including cosine filtering, Gaussian processes, and polynomial fits) or provide their own set of detrended light curves via methods of their choosing. The **democratic detrender** then combines the resulting individually detrended light curves into a single method marginalized (via median selection) light curve. Additionally, the **democratic detrender** inflates the uncertainties of each time-series data point using information from the median absolute deviation between the individually detrended light curve, propagating information into the final detrended light curve about the added uncertainty due to the correctness of the underlying models.

1. INTRODUCTION

Space-based stellar time-series photometry shows a combination of periodic, quasi-periodic, and non-periodic variations caused by both physical and observational factors. As discussed in a series of papers studying the noise properties in *Kepler* time-series photometric data (e.g., Jenkins et al. 2010; Gilliland et al. 2010, 2011, 2015), there are four predominant components that together make up the observed variability: (1) detector noise, (2) stellar activity, (3) spacecraft motion, telescope, & instrumental induced variations, and (4) the eclipses or transits of interest.

Detector noise is non-periodic noise driven by random fluctuations in the detector and is typically assumed to be white noise. Stellar activity is a quasi-periodic phenomenon caused by fluctuations on the stellar surface. There are certain phenomena that on short timescales are largely periodic, such as star spots with a period equal to the rotational period of the star, and other phenomena, such as stellar flares, that are not expected to be periodic. Additionally, stellar photometry will always have some intrinsic Poisson noise that cannot be removed from the time-series light curves (Angus et al. 2017). Spacecraft, telescope, & instrument noise can be both period and non-periodic. Events such as momentum dumps for course correction happen on a periodic basis, but sudden changes caused by motion of the spacecraft, instrumental issues, or telescope issues do not follow a periodic schedule (e.g., Borucki et al. 2010; Ricker et al. 2015). Lastly, the eclipse or transit event will be periodic, as a single transit event occurs once per orbit

Corresponding author: Daniel A. Yahalomi
daniel.yahalomi@columbia.edu

* LSST-DA DSFP Fellow

† Harvard SRMP Student

of the planet. Stable planetary orbits will be purely periodic, albeit with minute fluctuations (or transit timing variations). An illustration of how these four different components contribute to space-based stellar time-series photometry can be seen in Figure 1.

As discussed in Hippke et al. (2019), in the last decade, millions of light curves have been provided to the community thanks to space-based instruments such as *CoRoT* (Auvergne et al. 2009), *Kepler* (Borucki et al. 2010), *K2* (Howell et al. 2014), *TESS* (Ricker et al. 2015), and *CHEOPS* (Benz et al. 2021). In the coming decade, this number will continue to grow, with future space-based time-series missions such as *PLATO* (Rauer et al. 2014), *Nancy Grace Roman Space Telescope* (Spergel et al. 2015), and *Earth 2.0* (Ge et al. 2022). Ground based facilities, such as *KELT* (Pepper et al. 2007), *WASP* (Pollacco et al. 2006), and *HATnet* (Bakos et al. 2004), have additionally contributed enormously to our wealth of time-series photometry and will continue to do so in the coming decade with instruments such as the *Vera C. Rubin Observatory* (Ivezić et al. 2019) coming online.

In modeling time-series photometry, particularly for short baseline eclipse events such as transiting exoplanets, eclipsing binaries, and self-lensing binaries, accurately and precisely removing coherent photometric variations is a critical step in correctly modeling the eclipse event. In response to the abundance of time-series data made available in the last decade many different modeling algorithms and techniques have been used for fitting out-of-transit trends in the light curves and removing these trends from the light curve – this process will henceforth be called detrending (and is sometimes also referred to as pre-whitening) (e.g., Mazeh et al. 2007; Kim et al. 2009; Mazeh & Faigler 2010; Ofir et al. 2010; Fabrycky et al. 2012; Gautier et al. 2012; Vanderburg & Johnson 2014; Waldmann 2014; Aigrain et al. 2016; Luger et al. 2016; Angus et al. 2017; Sandford & Kipping 2017; Giles et al. 2018; Luger et al. 2018; Hippke et al. 2019; Morvan et al. 2020; Hattori et al. 2022; McGruder et al. 2022). While many of these detrending methods have been found to work quite well in practice, from a theoretical standpoint they are by definition imperfect as they are all misspecified models. This is not a failure of the community to produce a “perfect” detrending models, but rather unfortunately the reality intrinsic to modeling stellar time-series photometry that is comprised of different periodic, quasi-periodic, and non-periodic components. This combined nuisance signal is so complicated that it is simply not solvable by any single detrending model.

Precise and accurate detrending becomes even more critical when searching for transient events (e.g., exomoon transits) where one has to be especially careful to neither remove nor add the subtle signatures of the transient event that, unlike exoplanet transits, will not phase-fold nicely on the planetary period and thus one cannot expect morphological repetition (Teachey & Kipping 2018). A schematic example of detrending can also be seen in Figure 1.

The **democratic detrender** is written to be used with a method of transit fitting in which one models the transit in two steps: (1) modeling and removing unwanted activity and (2) fitting a transit to the detrending dataset.

One might wonder about the alternative (but often computationally expensive) approach of jointly fitting, since our two-step approach admittedly has the disadvantage of assuming a perfect removal of unwanted activity in the subsequent transit modeling. We mitigate somewhat for this in the **democratic detrender** by inflating the uncertainties by the variance between the different detrending models. In practice, this two-step method is only appropriate to use when the baseline of out-of-transit data greatly exceeds the baseline of in-transit data, a typical situation for transit surveys. This is because in the two-step method, one masks the in-transit data, trains (fits) the detrending models on the out-of-transit data, and then interpolates the detrending models over the in-transit times. As *Kepler* and *TESS* observe quarters or sectors for \sim month-long time periods, data from these missions are ideal for this method of detrending they consistently have very long out-of-transit baselines. In contrast, if modeling a transit with a short baseline of data, such as typical *JWST* or *Hubble* observations, one would be better advised to model the nuisance signal in unison with the transit model. Additionally, when modelling *K2* data one would be better off using a detrending method explicitly designed to account for the large effects of the frequent thruster firings – two of the most commonly used algorithms is the self-flat-fielding (SFF) presented in Vanderburg & Johnson (2014) and the EVEREST package (Luger et al. 2016, 2018).

In three of the four detrending models (excluding the **local** model) used in the **democratic detrender** by default there is an emphasis on fitting low frequency (long period) noise and ignoring high frequency (short period) noise. This is so that we will not distort the transit shape with non-physical high frequency noise (Waldmann et al. 2012). Additionally, this decreases the chance of either hiding or erroneously adding moon-like transit dips – i.e., minimizes both the false negative

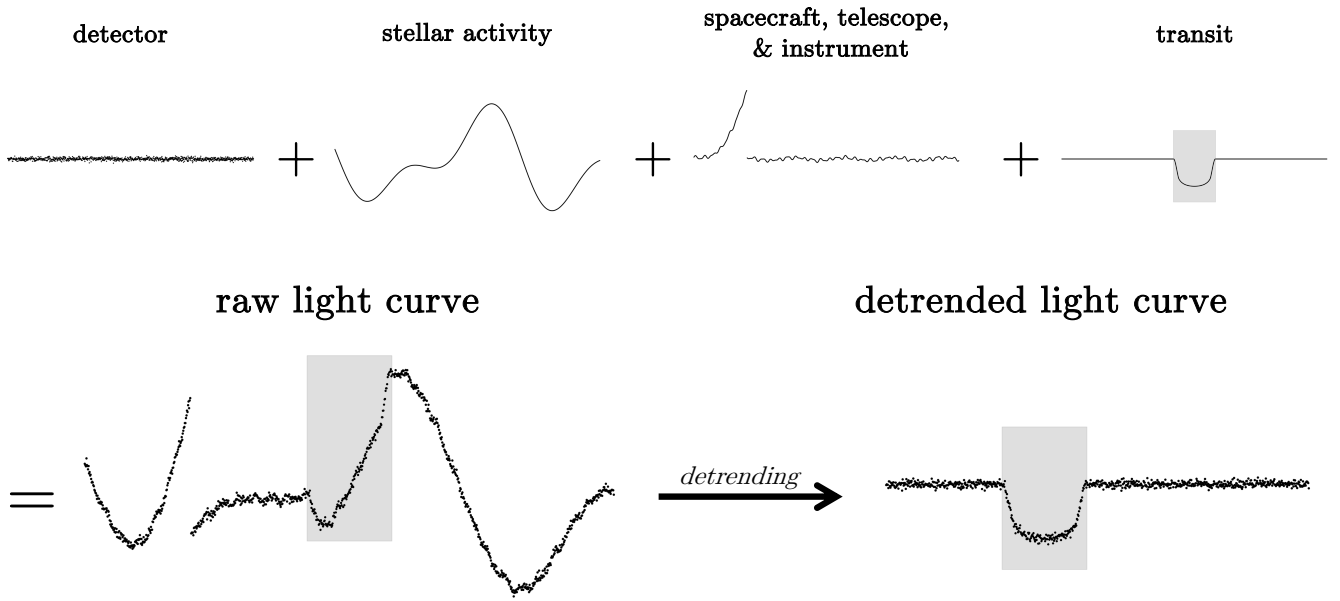


Figure 1. The four primary contributions to space-based stellar time-series photometric data are (1) detector noise, (2) stellar activity, (3) spacecraft motion, telescope, & instrumental induced variations, and (4) eclipses or transits. Detrending is the process of removing as much of the stellar activity and spacecraft, telescope, & instrument noise (i.e., “nuisance signal”) as possible without adding additional non-physical features.

and false positive rates. For *Kepler* and *TESS* data, where we will frequently have multiple transit epochs, we would not expect high frequency noise to be coherent with the transits (Pont et al. 2006). Thus by including multiple transits this incoherent high frequency noise should essentially cancel itself out, scaling with \sqrt{N} transit epochs. In this context, the boundary between high frequency and low frequency noise is defined at a frequency commensurate with the transit duration. In what follows, in Section 2 we present the theory behind ensemble-based detrending via a community of models. Then, in Section 3 we outline the detrending methods implemented by default in the **democratic detrender**, its modularity, and its customizability – and walk through an example case of detrending a light curve with the **democratic detrender**. The source code can be found on GitHub.¹ Tutorials and API documentation can be found on Read the Docs.²

2. ENSEMBLE METHODS

2.1. Ensemble Learning

As there exists no perfect detrending models, we adopt an approach similar to the common machine learning technique of ensemble learning, where a community of networks each classify a dataset and then the final result is a combination of the individual classifiers. Ensemble learning systems have become increasingly useful tools to improve the accuracy of automated decision-making systems (Zhang & Ma 2012). The underlying idea is that by aggregating the predictions of a group of models, one can often achieve better results than any single model could alone. As noted in Zhang & Ma (2012), while ensemble-based decision making in machine learning is a relatively new concept of the past several decades (Dasarathy & Sheela 1979; Hansen & Salamon 1990; Schapire 1990), ensemble-based decision making is a fundamental manner in which humans have made decisions for as long as civilized communities have existed. Mirroring the fundamental philosophy behind democracy, in which decision is made via a vote of the people, ensemble-based decision making is a process in which the final model values are decided via a “vote” of a set of included independent models.

Ensemble methods take advantage of the fact that the modeling error is composed of two components: bias (accuracy of the model) and variance (precision of the

¹ https://github.com/dyahalomi/democratic_detrender

² <https://democratic-detrender.readthedocs.io/en/latest/>

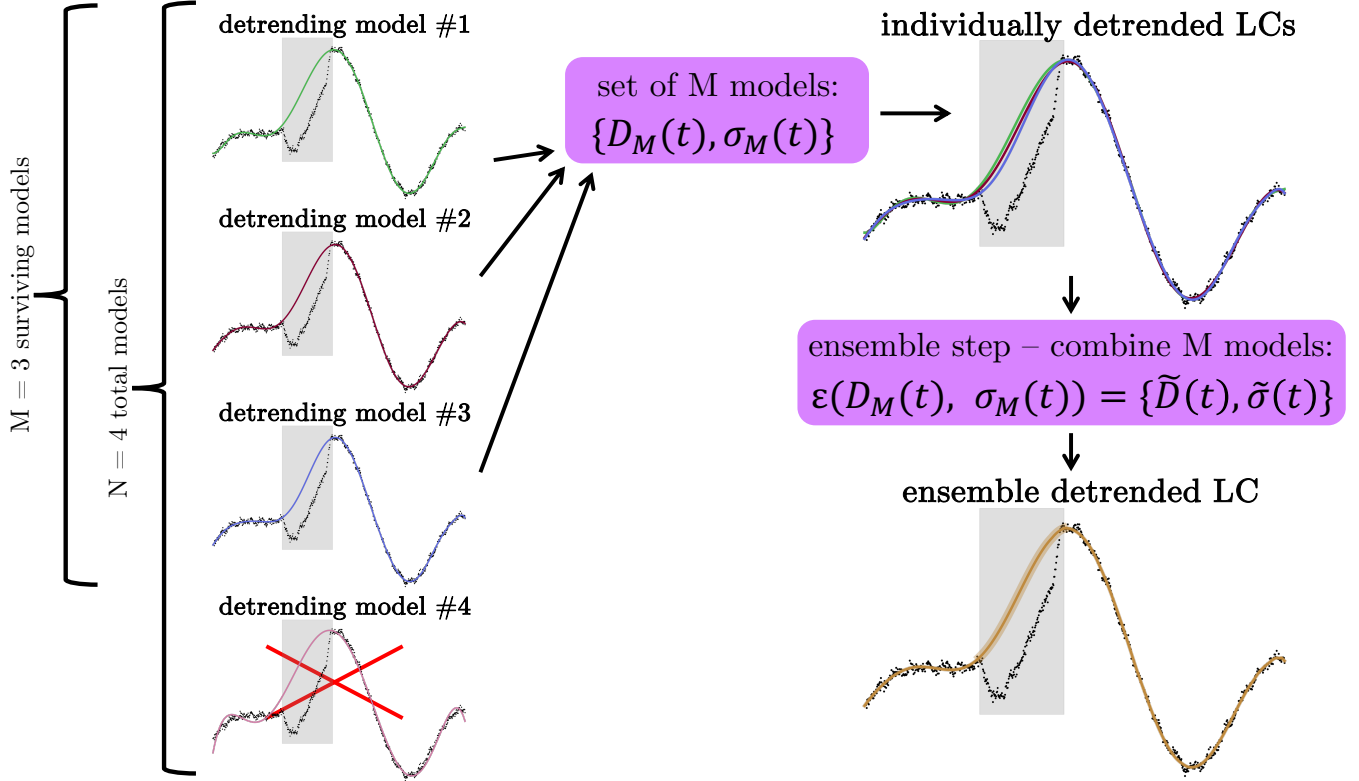


Figure 2. An example of ensemble detrending in practice. Here we’ve taken the simulated light curve (LC), presented in Figure 1 and fit the non-transit data with four different detrending methods. Detrending model #4 failed to accurately fit the data, and thus would fail the tests of Gaussianity and be removed before the ensemble step. In the top right one can see that detrending with each of the three individual detrended methods can result in noticeably different predictions for the transit shape. In the ensemble detrended light curve in the bottom right, we take the median detrended solution for each data point, as described in Equation 1. Additionally, we inflate the error bars, as shown by the shaded region in the ensemble detrended LC, by adding in quadrature the reported errors with the median absolute deviation between the different detrending methods, as described in Equation 2. In total, the ensemble step is thus described by Equation 3.

model) (Zhang & Ma 2012). By using several independent classifiers with relatively similar accuracy, and then combining the outputs via i.e., averaging or median-selection, one can increase the precision of the overall solution by smoothing the results. Here in lies two points worth noting with ensemble decision making methods (1) there exists a choice to be made on how to combine the different detrending methods – the voting system and (2) combining several detrending methods doesn’t guarantee a detrending fit that outperforms each of the input detrending methods, but rather it reduces the likelihood of selecting a detrending method with a poor or biased performance (Zhang & Ma 2012).

2.2. Ensemble Detrending

In general, each of the individual detrending models are equally valued by the community, and so we have no reason to weight any models more than others. Additionally, as we want to exclude outliers from strongly influencing our detrended light curve values, we adopt a median selection for our ensemble voting step. We addi-

tionally inflate the uncertainties in our final detrending light curve based on the variance between the different detrending methods – allowing us to propagate information on the agreement between the different independent models. A schematic of ensemble detrending can be seen in Figure 2.

In order to not bias the detrending results, we emphasize that it is important to include orthogonal detrending models into the ensemble step of detrending. For example, one wouldn’t want to pass multiple polynomials of different orders into the ensemble detrender as these are non-orthogonal detrending models and thus one would be essentially giving more weight to polynomial fits in the ensemble detrending light curve. The goal of ensemble detrending is to mitigate for model-dependent imperfections in the detrending, and so by using disparate detrending methods, one decreases the likelihood of biasing the final result.

Assuming we start with N total models for the stellar activity per transit epoch, similar to Kipping et al. (2022), we first test the Gaussianity of each of the N

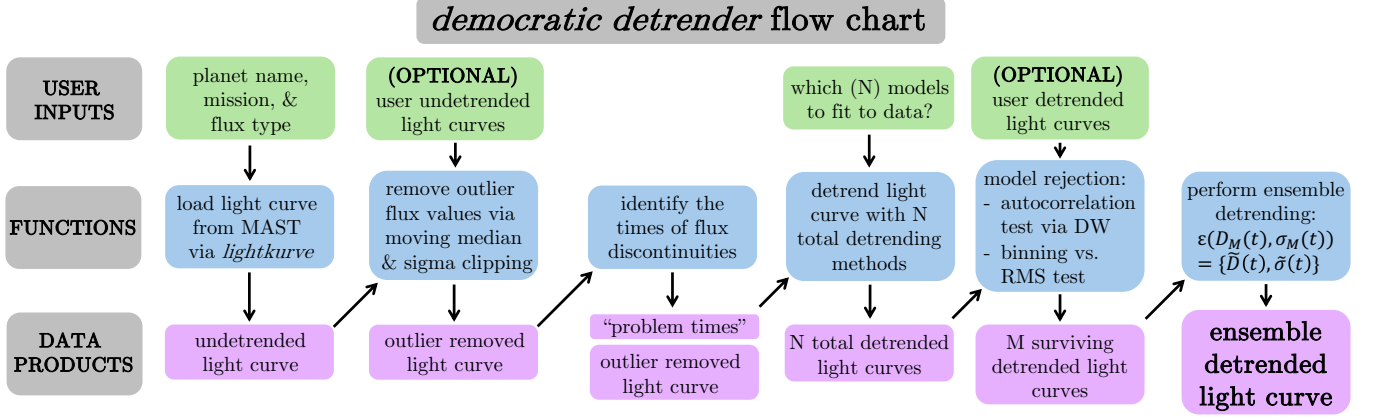


Figure 3. Flow chart depicting required and optional user inputs, built-in functions, and output data products for the **democratic detrender**. As long as the user passes in the requisite inputs and data products, the **democratic detrender** can be initiated at any of the intermediate functions. This flow chart thus displays the modularity and customizability of the **democratic detrender**.

individually detrended light curves in two ways: (1) autocorrelation test at a timescale of the data’s cadence via the Durbin-Watson statistic and (2) Poisson counting of independent measures test via binning vs. root-mean-square metric. These tests are described in much more detail in Section 3.5. Once we remove anomalous ($> 3\sigma$ outliers) detrending models, we are then left with M ($\leq N$) surviving detrending models per epoch. We note that this 3σ cutoff removing the complete epoch of any detrending model that shows non-white noise properties – rather than a point-by-point removal of $\sim 0.3\%$ of the data. Here the priority is ensuring that we only pass white light curves into the final ensemble step, even if this means having less M final detrended light curves.

If $D_M(t)$ is the M ’th detrending model D ’s light curve at time t , then our corresponding democratically detrended light curve \tilde{D} at time t is:

$$\tilde{D}(t) = \text{median}_{m=1,\dots,M} \{D_m(t)\} \quad (1)$$

Additionally, in ensemble detrending as implemented in the **democratic detrender**, we propagate the variance between the different detrending methods by adding in quadrature for each i ’th data point the uncertainty on the flux input by the user by the median absolute deviation (MAD) of the different model predictions multiplied by a factor of 1.4286 (Teachey & Kipping 2018). If $\sigma(t)$ is the error on the flux value at time t then the ensemble detrended error, $\tilde{\sigma}(t)$ would be:

$$\tilde{\sigma}(t) = \sqrt{[\sigma(t)]^2 + [1.4286 * \text{MAD}_{m=1,\dots,M} \{D_m(t)\}]^2} \quad (2)$$

Thus in total, $\epsilon(D_M(t), \sigma_M(t))$, the “ensemble” function of the **democratic detrender**, takes a set of M individually detrending light curves and uncertainties and

combines them into a single ensemble detrended light curve by both taking the median value at each time, t (see Equation 1), and also inflating the uncertainties by the variance between the surviving M detrending models (see Equation 2):

$$\epsilon(D_M(t), \sigma_M(t)) = \tilde{D}(t), \tilde{\sigma}(t) \quad (3)$$

This outlines the fundamental theory behind ensemble detrending (previously also referred to as method marginalized detrending (Teachey & Kipping 2018) and democratic detrending (Yahalom et al. 2024)) as implemented in the **democratic detrender**.

3. DEMOCRATIC DETRENDER

In what follows, we demonstrate the workflow of the **democratic detrender**, as also shown in Figure 3. We will use Kepler-1519 b as a sample detrending target, demonstrating each step of the **democratic detrender**. Kepler-1519 b is a cool gas giant on a ~ 240 day orbit. It was identified as a target of interest in Kipping & Yahalom (2023) as it shows short-period transit timing variations (TTVs) that could be consistent with either moon or a companion, non-transiting planet. We highlight that while we use a *Kepler* target as our example, this code has also been extensively tested on *TESS* datasets as well (Kipping et al. 2024, submitted).

3.1. Load Raw Light Curve

The first step is loading in the raw light curve. The **democratic detrender** is setup to load light curves from NASA’s Space Telescope Science Institute (STScI) Barbara A. Mikulski Archive for Space Telescopes

(MAST)³ via the `lightkurve` package (Lightkurve Collaboration et al. 2018).

The user must only supply a stellar ID and a planet number. The user need not supply a specific type or format ID, as the `democratic detrender` queries the SIMBAD Astronomical Database – CDS (Strasbourg)⁴ to find the corresponding TIC ID. If this fails for any reason, the `democratic detrender` then tries to query NASA’s Exoplanet Archive⁵ to find the relevant TIC ID. For example, for Kepler-1519b, the user could supply any of the following IDs, and the `democratic detrender` would function exactly the same: 2MASS J19464029+4927426, AP J19464029+4927426, Kepler-1519, KIC 11518142, KOI-3762, LAMOST J194640.29+492742.6, TIC 351191596, Gaia DR2 2086851495906130176, and Gaia DR3 2086851495906130176.

With the appropriate TIC ID in hand, the `democratic detrender` then queries NASA’s exoplanet archive in order to load in the planet’s period, transit duration, and time of transit midpoint. This information is used when detrending in order to generate the transit mask. The user can optionally supply their own period, transit duration, and/or time of transit midpoint if they so choose.

Next, the `democratic detrender` loads in the light curve (set of times, flux values, and flux uncertainties) from MAST via the `lightkurve` package (Lightkurve Collaboration et al. 2018). The user must supply what type of flux data to load, be it Simple Aperture Photometry (SAP) or Pre-search Data Conditioning SAP (PDCSAP). For *TESS* data one can additionally query QLP (Quick Look Pipeline) data. By default, the `democratic detrender` will load in short cadence data, if it exists, and will only use long cadence data if short cadence observations don’t exist for a specific target.

In general, we recommend users to use both SAP and PDCSAP data. This is because PDCSAP data runs the risk of being over-corrected if too many cotrending basis vectors are used. By using both the “raw” SAP data and the PDCSAP data, one can reduce the likelihood of removing signal from the data before fitting for transits or other signals in the time-series photometry.

A transit mask is then created, to mask all transits in the data. By default, we mask $1.1 t_{\text{dur}}$ where t_{dur} is the input transit duration. We do this in order to account for possible transit timing variations (TTVs) in

the dataset. This transit duration multiplicative factor can be customized to the user’s preference.

PDCSAP data is provided to the community already corrected using a contamination factor, called “CROWDSAP” in the header, and a flux fraction, called “FLFRSAP”. CROWDSAP represents the quarterly-averaged ratio of the target flux to the total flux in the photometric aperture and is a scalar value between zero and unity. FLFRSAP is the quarterly-averaged fraction of light coming from the optimal aperture used in the SAP data and is a scalar between zero and unity. These two factors are then used in correcting the PDCSAP data via the following equation (Stumpe et al. 2012; Smith et al. 2012):

$$\tilde{y}(t) = \frac{y(t) - (1 - c) * \text{median}(y(t))}{f} \quad (4)$$

where $\tilde{y}(t)$ is the corrected cotrended flux values, $y(t)$ is the cotrended flux values, c is the CROWDSAP crowding metric, and f is the FLFRSAP flux fraction metric.

Some of this blend data may not include the most recent information, especially with new data from *Gaia*⁶ (Gaia Collaboration et al. 2016) and the SAP data does not contain this correction. Therefore, by default, we remove this blend correction from the PDCSAP data following (Kipping & Tinetti 2010) where $c = 1/\mathcal{B}$ and \mathcal{B} is the blend factor

$$\mathcal{B} = \frac{F_* + F_{\text{blend}}}{F_*} \quad (5)$$

The provided corrected PDCSAP flux values will equal F_* and we want to solve for the $F_{\text{total}} = F_* + F_{\text{blend}}$. Thus, we can do so by dividing the provided F_* values by the quarter-averaged CROWDSAP values – yielding the uncorrected PDCSAP flux values. These uncorrected $y(t)$ values are what we adopt for our PDCSAP data, by default. However, this process of removing the blend factor can be turned off, and the *Kepler* provided corrected PDCSAP flux values can be used.

Finally then, the raw, undetrended light curve (set of times values, flux values, and flux uncertainties) as well as relevant metadata is returned.

Currently, the `democratic detrender` is only setup to query and load *Kepler* or *TESS* lightcurves. However, a user can always provide their own raw undetrended LC.

3.2. Remove Outlier Flux Values

³ <https://archive.stsci.edu/>

⁴ <https://simbad.u-strasbg.fr/simbad/>

⁵ <https://exoplanetarchive.ipac.caltech.edu/>

⁶ <https://www.cosmos.esa.int/web/gaia>

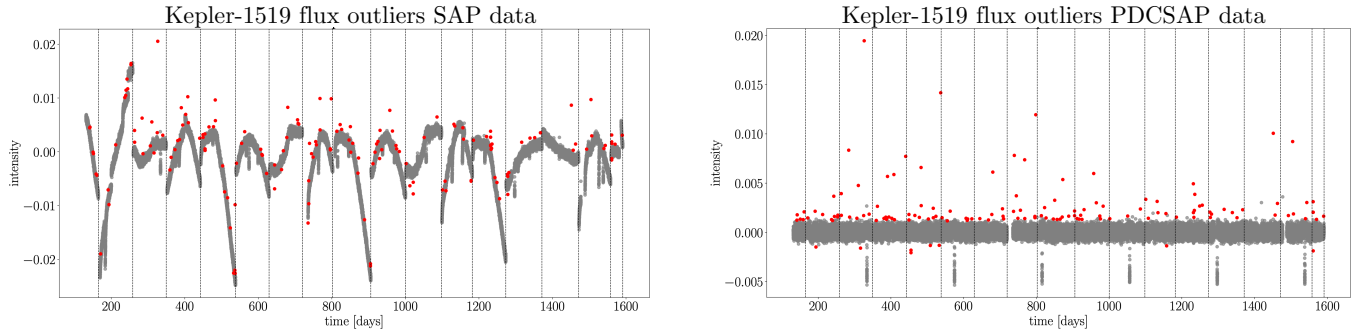


Figure 4. Raw (not detrended) SAP [left] and PDCSAP [right] light curves for Kepler-1519 b. Red data points are those that were deemed outliers via moving median rejection and thus removed from subsequent modeling. The grey dotted lines show the different *Kepler* quarters in the data.

Now we begin the process of manipulating the time-series photometry. The first step is to remove outlier flux values. By default, we do so via sigma clipping any flux values in the out-of-transit data that are more than 4σ anomalies in a moving median for a time window of 30 cadences (these default selections for sigma clipping can also be adjusted by the user). Outlier rejection via sigma clipping can also be turned off. This can be advisable for short cadence *Kepler* datasets or short cadence *TESS* datasets with many sectors of observations, where this process becomes computationally expensive.

Once outlier rejection is completed, Figure 4 is automatically generated. Here the vertical dashed lines represent the quarters, the grey dots represent the non-outlier flux values, and the red dots represent the outlier, and thus removed, values.

3.3. Identify Times of Flux Discontinuities

Detrending models will gain no information on the underlying variability from random variations in the light curve. Further, random (i.e., non-periodic) variations can worsen the accuracy of the detrending models. As explained previously and demonstrated in Figure 1, the spacecraft, telescope, & instrument (and even in some cases stellar activity such as stellar flares) can create flux discontinuities. Additionally, these discontinuities can cause detrending models to fail, by forcing the models to try to account for sudden extreme variations. As such, we must remove these discontinuities from the data before detrending. Labeling flux discontinuities is particularly important for using SAP data, where these discontinuities are very prevalent, but it is also good practice for the PDCSAP data. By default, if the user does not label PDCSAP discontinuities, the **democratic detrender** will assume that there are none. However, if SAP flux discontinuities are identified, the user can choose to use the SAP times of discontinuity for the PDCSAP data as well.

The data is automatically split into quarters (for *Kepler* data) or sectors (for *TESS* data). In between successive quarters or sectors of observation, the target star cannot be expected to fall exactly on the same location in pixel space of the telescope, and so we split the data by quarters or sectors to remove any bias this could introduce into the detrending.

The user must then look through the data and identify flux discontinuities, to be removed from the data. We note that discontinuities only in time space (data gaps that don't correspond with flux jumps) do not need to be labeled as a discontinuity. Identification and labeling of discontinuities can all be done in the **democratic detrender**, using a built in GUI with sliders that allows the user to identify and save the set of flux discontinuities in the data. An example of the times the user would want to label as discontinuities to be removed from the data can be seen in Figure 5

3.4. Detrend Light Curves

Finally, with all this data cleaning completed, we can detrend our time-series photometry. As previously stated, there are a number of common detrending used by the astronomy community. By default, the **democratic detrender** uses four different fitting techniques: (1) GP, (2) **polyAM**, (3) **CoFiAM**, and (4) **local**. These four detrending techniques are applied to both the PDC and SAP time-series photometry, for a total of $N=8$ individually detrended light curves. An example of these $N=8$ individually detrended light curves for Kepler-1519 b can be seen in Figure 6. This figure is also auto-generated by the **democratic detrender** when detrending completes.

Each of these four detrending models have been used extensively in exoplanet literature, but a brief summary, in part adapted from [Yahalomi et al. \(2024\)](#), can be seen below:

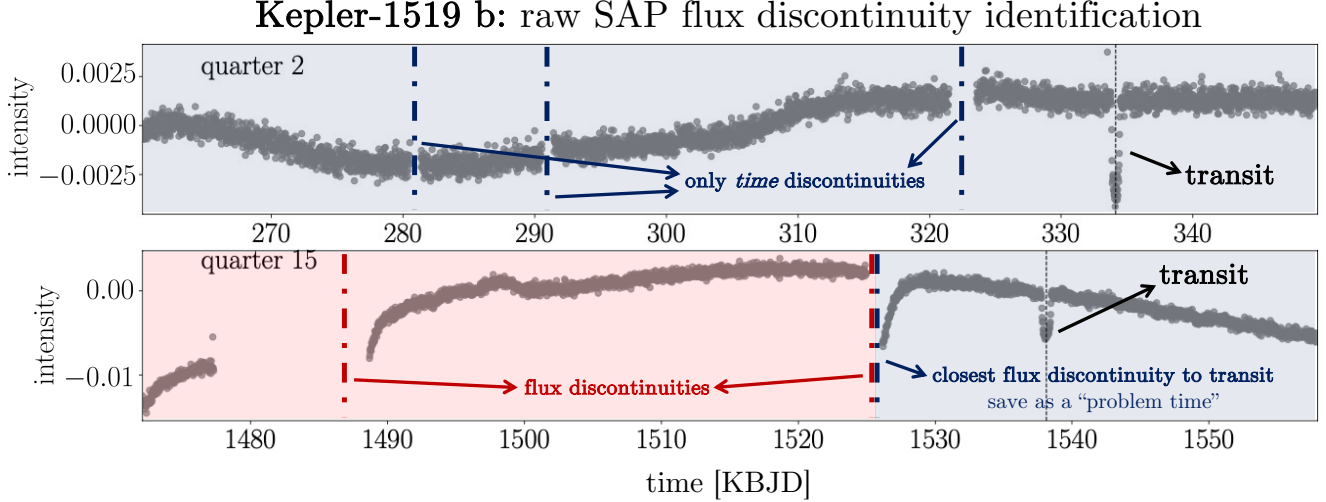


Figure 5. The top row is Kepler-1519b’s 2nd quarter of SAP data. In the 2nd quarter we can see that there are 3 time discontinuities, but as these time gaps don’t coincide with a flux intensity discontinuity as well, we wouldn’t want to remove any of the data from our detrending. The bottom row is Kepler-1519b’s 15th quarter of SAP data. In the 15th quarter, we can see that there are 2 flux intensity discontinuities that coincide with time discontinuities. In this case, we would want to label the closest flux discontinuity to the transit (KBJD ~ 1527). Once we label this problem time, the democratic detrender will clip the data here, and remove all data from earlier in the quarter, before fitting the detrending models.

- **CoFiAM:** Cosine Filtering with Autocorrelation Minimisation was first presented in [Kipping et al. \(2013\)](#) and builds on cosine filtering approach used to study CoRoT data ([Mazeh & Faigler 2010](#)). Specifically, the out-of-transit time-series photometry is regressed over using a high-pass, low-cut filter via a discrete series of harmonic cosine functions, with the functional form given by

$$f_k(t) = a_0 + \sum_{k=1}^{N_{\text{order}}} \left[x_k \sin\left(\frac{2\pi tk}{2D}\right) + y_k \cos\left(\frac{2\pi tk}{2D}\right) \right]. \quad (6)$$

Here, D is the total baseline of the time-series data in a given epoch, t is the set of observing times in the epoch, x_k and y_k are free parameters in the model, and N_{order} is the highest allowed harmonic order. The selection of N_{order} is important, because above a certain limiting threshold, harmonics with a similar timescale as the transit can distort the transit profile. In order to determine N_{order} , we train 30 models (above which numerical instabilities arise), where N_{order} ranges from 1 to 30, and at each epoch pick the cosine filter that leads to the least correlated light curve via the Durbin-Watson statistic ([Durbin & Watson 1950](#); [Kipping et al. 2013](#)).

- **GP:** In this detrending technique, we fit a Gaussian Process to the out-of-transit time-

series photometry using the quasiperiodic kernel presented in [Angus et al. \(2017\)](#) as a reliable model for stellar activity of a rotating star. Specifically, we use a SHOTerm kernel from `celerite2` via the `exoplanet` package, which is a stochastically-driven, damped harmonic oscillator (`exoplanet`, [Foreman-Mackey et al. 2021](#)), (`celerite2`, [Foreman-Mackey et al. 2017](#); [Foreman-Mackey 2018](#)).

- **polyAM:** Polynomial detrending with Autocorrelation Minimisation follows a similar process to CoFiAM, except we train 30 models with polynomials as the basis function. Polynomial filtering is a common method for stellar activity detrending (e.g., [Fabrycky et al. 2012](#); [Gautier et al. 2012](#); [Giles et al. 2018](#)). In polyAM, the 30 different bases models are 1st- to 30th-order polynomials. For each epoch, as in CoFiAM, the least correlated light curve via the Durbin-Watson statistic ([Durbin & Watson 1950](#)) is chosen.
- **local:** The local polynomial detrending technique again uses 1st- to 30th order polynomials, but the order of the polynomial is selected via the lowest Bayesian Information Criterion ([Schwarz 1978](#)) computed on the data within six transit durations of the time of mid-transit. This a fairly typical detrending method for the analysis of short-period transits ([Sandford & Kipping 2017](#)).

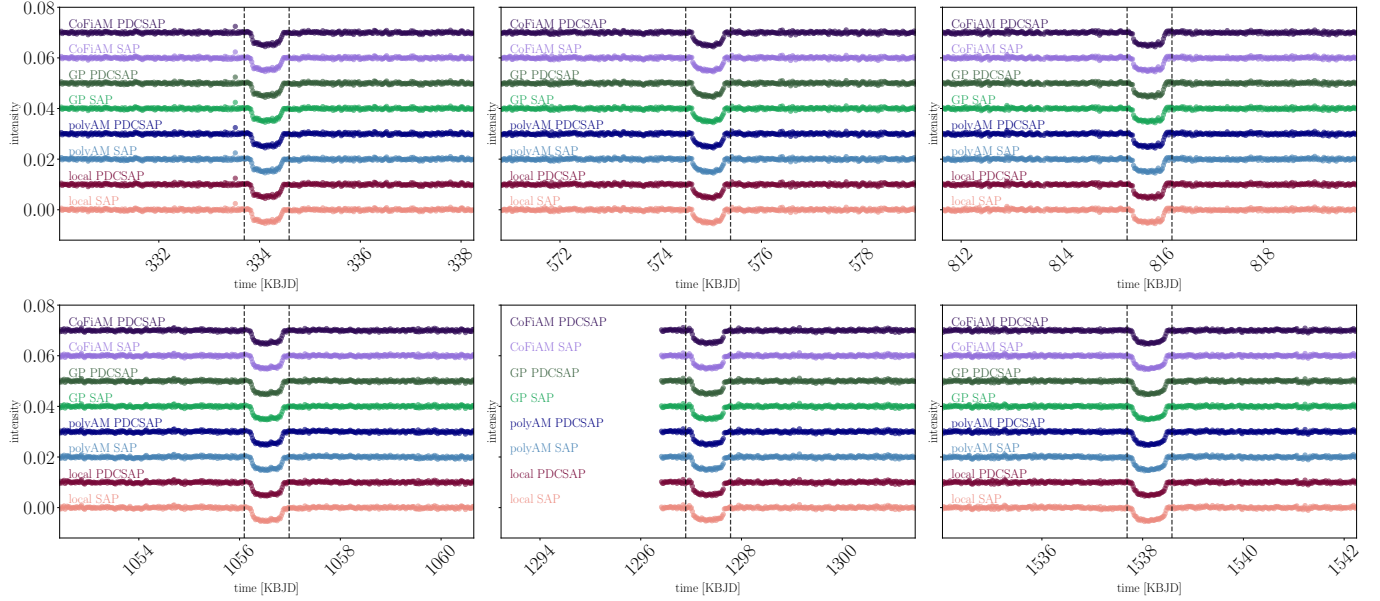


Figure 6. Individually detrended light curves for Kepler-1519 b. Included in this figure are all 8 default detrending methods in the **democratic detrender**, which are CoFIAM, GP, polyAM, local run on both the SAP data and PDCSAP data. The vertical dashed lines show the in-transit portion of the light curve (LC) that was “masked” and thus not included in the model fitting process. Instead for these portions of the LC, the model fit is extrapolated from the rest of the out-of-transit data such that physical transit features are not removed unintentionally.

As stated in Section 1, there are many different detrending models used by the exoplanet community to detrend time-series stellar photometry. Therefore, it is likely that there are potential users of the **democratic detrender** that would like to use a detrending model not provided by the **democratic detrender**. For example, the Tukey’s biweight algorithm, popularized by the *Wotan* package and Hippke et al. (2019) that demonstrated its utility in modeling stellar time-series photometry is not a detrending model built into the **democratic detrender**. A tutorial notebook showing how one can include a new detrending model, in this case Tukey’s biweight, can be found on the Read the Docs.⁷

Therefore, we have made an optional argument in our code to accept any additional user supplied detrended light curves, to be included in all subsequent steps. Additionally, the user can decide which of the 4 included detrending models to use in their detrending.

We again emphasize the important of choosing orthogonal and independent detrending models. One might notice that of the included detrending models, CoFIAM and polyAM both select the order of the basis function via autocorrelation minimization, but as the basis functions in these two methods are quite different, these models are still quite orthogonal. Additionally, polyAM and local both fit polynomials to the LCs, however they are

trained on different subsets of the data and the method in which the order of the polynomial selected is different.

3.5. Model Rejection

We now have by default $N=8$ individually detrended light curves produced by the **democratic detrender** and any user supplied individually detrended light curves. The SAP datasets, PDCSAP datasets, and user supplied detrended LCs could have the same or slightly different time arrays in the datasets. This is because it is possible that with discontinuity identification certain portions of the dataset are removed from SAP data, but not from PDCSAP data, for example. So before we can aggregate these light curves together via the ensemble step, we must make them all have the same exact time values. In order to do so, we pad the flux and flux uncertainty sets with a *NaN* value for any time that is missing in a given individually detrended dataset.

For each of the N individually detrended light curves, we want to test the Gaussianity of each detrending model for each epoch. To this end, we perform two bootstrapping tests via Monte Carlo simulations: (1) a test of the autocorrelation of the detrended flux values via the Durbin-Watson (DW) statistic and (2) a test of excess noise in the light curve via the binning vs. root-mean-square variance expected behavior. This allows us to remove non-Gaussian and autocorrelated detrended LCs before the ensemble step.

1. Autocorrelation test via DW metric:

⁷ <https://democratic-detrender.readthedocs.io/en/latest/>

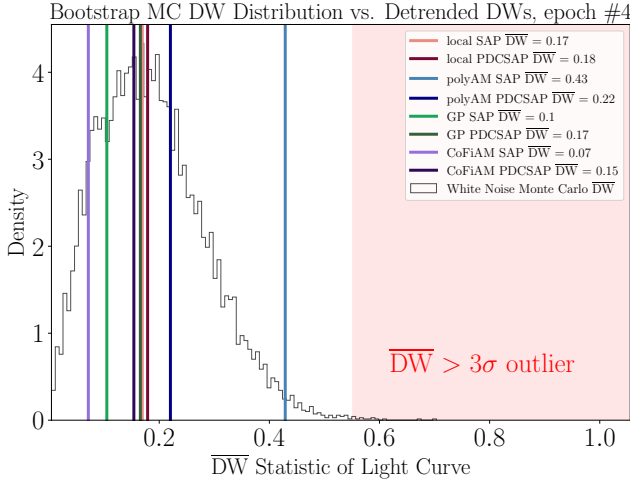


Figure 7. Bootstrapping test of autocorrelation via the DW metric for Kepler-1519 b’s 4th transit epoch. The histogram shows the Monte Carlo results for a slightly modified DW metric, \overline{DW} , as defined by Equation 8 for simulated white noise with the same uncertainties as the light curve. The vertical lines show the \overline{DW} values for each of the 8 detrending models. Shaded in red are \overline{DW} values that are more than $3\text{-}\sigma$ outliers. Any detrending model that falls in this shaded region is excluded from the final ensemble detrended model.

The Durbin-Watson (DW) statistic, as first presented in [Durbin & Watson \(1950\)](#), is a metric used that can be used to detect autocorrelation, or the correlation of a signal with a delayed copy of itself, in time-series analysis. In our context, DW is defined as

$$DW = \frac{\sum_{t=2}^T (e_t - e_{t-1})^2}{\sum_{t=1}^T e_t^2} \quad (7)$$

where e_t is the residual at time t . The value of the DW statistic ranges from 0 to 4, where DW of 2 means no autocorrelation.

As implemented here (as can be seen by the e_{t-1} term in Equation 7), DW is the lag one autocorrelation with the timescale of the cadence. In order to use a different timescale (e.g., an hour) one would have to first bin the time series to that cadence.

If the data was infinitely long, then we would expect the DW statistic of a detrended dataset to approach 2. As our dataset is finite, instead we can perform a bootstrap test of the DW statistic for each individually detrended LC at each epoch by creating a Monte Carlo (MC) simulation with 10,000 realizations of random Gaussian noise with

a standard deviation equal to the provided flux uncertainties.

We then determine the DW statistic for each of the 10,000 MC realizations using Equation 7. As there is a significant datagap at each transit, we determine the DW statistic for the pre-transit and post-transit data separately and then combine them by adding in slightly modified quadrature as follows

$$\overline{DW} = \sqrt{(DW_{\text{pre}} - 2)^2 + (DW_{\text{post}} - 2)^2}. \quad (8)$$

For the \overline{DW} statistic, a dataset with no autocorrelation will have a value of 0.

We can then use the inverse error function to determine the location of the $3\text{-}\sigma$ upper bound limit by identifying the 99.7th percentile of the DW statistic from the Monte Carlo simulations. Then we determine the \overline{DW} statistic for each individually detrended light curve at each epoch, and remove any individually detrended epochs that are more than $3\text{-}\sigma$ outliers. As \overline{DW} will never be less than zero and a \overline{DW} value closer to zero is indicative of a dataset that shows less autocorrelation, there is only a $3\text{-}\sigma$ upper bound. See Figure 7 for an example of the autocorrelation via DW test for a sample epoch of Kepler-1519 b. The sigma cutoff parameter is customizable (e.g., users can change the cutoff to be a stricter $2\text{-}\sigma$ upper bound) if they want to be more or less strict on what is considered an outlier.

2. Binning vs. RMS test:

We also run a “time-averaging” test of correlated red noise that was first propounded in [Pont et al. \(2006\)](#) and we follow closely to the formalism described in detail in [Carter & Winn \(2009\)](#). In short, we determine the standard deviation of both the unbinned data, $\hat{\sigma}_1$, and also the time averaged data, $\hat{\sigma}_n$ where every n points have been averaged (thus creating m time bins.) In the absence of correlated (red) noise, we expect white noise will behave as

$$\hat{\sigma}_n = \frac{\hat{\sigma}_1}{n^{1/2}} \left(\frac{m}{m-1} \right)^{1/2} \quad (9)$$

In the **democratic detrender** we use a minimum M_{bins} value of 1 data point and a maximum M_{bins} value equal to 1/10 the length of the total included dataset. For computational efficiency, we bin by index rather than time, and assume that

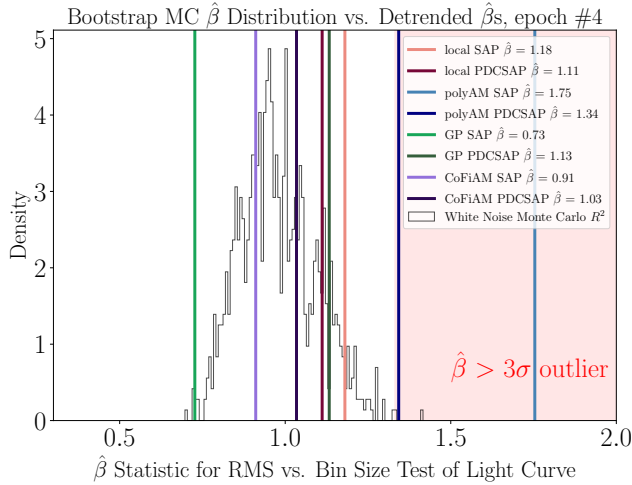


Figure 8. Bootstrapping test of root-mean-square (RMS) vs. bin for Kepler-1519b’s 4th transit epoch. The histogram shows the Monte Carlo $\hat{\beta}$ values (see 9 and the subsequent definition of $\hat{\beta}$). A larger $\hat{\beta}$ value indicates the presence of coherent (red) noise. The vertical lines show the $\hat{\beta}$ values for each of the 8 detrending models. Shaded in red are $\hat{\beta}$ values that are more than $3\text{-}\sigma$ outliers. Any detrending model that falls in this shaded region would be excluded from the final ensemble detrended model.

the data near transit is approximately uniformly spaced. As this is a bootstrap test, if this is not the case, the effect should be mitigated as we bin the same way for both the MC simulated data and the real detrending model data.

In the presence of correlated noise, we expect that there will be excess noise above the theoretical expression in Equation 9. We define a factor, $\hat{\beta}_n$, that represents the ratio between the observed standard deviation of the binned data, $\hat{\sigma}'_n$ and its white noise theoretical expression ($\hat{\beta}_n = \hat{\sigma}'_n / \hat{\sigma}_n$). We then define the estimator, $\hat{\beta}$, defined as the mean of all $\hat{\beta}_n$ values, which represents the amount of excess red noise in the data. A value of $\hat{\beta}$ that greatly exceeds 1 is indicative of a coherent red noise.

We start our bootstrap test by simulating 1,000 light curves for each epoch with random Gaussian noise with the provided flux uncertainties. We determine the $\hat{\beta}$ value for each of these Monte Carlo simulations. For this set of $\hat{\beta}$ values, we then determine the $3\text{-}\sigma$ boundary limit for each epoch using the inverse error function, as described above.

Finally, for each epoch of each individually detrended light curve, we calculate the $\hat{\beta}$ value and remove any individually detrended light curves $\hat{\beta}$ values that are larger than the $3\text{-}\sigma$ cutoff. A $\hat{\beta}$ that

is so small that it is a $3\text{-}\sigma$ outlier in the other direction is indicative that the errors are likely overestimated. As this isn’t indicative of coherent noise, we don’t remove detrending models with this behavior. See Figure 8 for an example of the binning vs RMS test for a sample epoch of Kepler-1519b. The sigma cutoff parameter is customizable (e.g., users can change the cutoff to be a stricter $2\text{-}\sigma$ upper bound) if they want to be more or less strict on what is considered an outlier.

As shown in Figure 7 and Figure 8, for the 4th epoch of Kepler-1519b, 8 of the 8 detrending methods pass the DW autocorrelation test and 6 of the 8 detrending methods pass the binning vs. RMS test. Therefore for the second epoch of Kepler-1519b, we have $M=6$ detrending models to pass into the ensemble function, and we will not include `polyAM SAP` or `polyAM PDCSAP` in our ensemble function for the 4th epoch.

For each epoch, there can be a different number of M detrending models that survive the detrending tests. Figure 9 shows the ensemble of individually detrended light curves for Kepler-1519b that pass both tests. Here we can see that by including $N > 1$ detrending models in our whitening step, we allow for robust tests of whiteness, as we down select to only the $M \leq N$ white detrended light curves.

3.6. Ensemble Step

Finally, now, we can perform the ensemble step as presented in Equation 3. We take the median value at each time step for the M surviving individually detrended light curves at each epoch, as described by Equation 1. Additionally, we inflate the uncertainties by the variance between the different M surviving models, as described by Equation 2. This is described in depth in Section 2. Doing so results in our final ensemble detrended light curve, as shown in Figure 10.

As a final test, we ensure that, for each epoch, the ensemble detrended light curve does not exhibit signs of correlated noise by again using the same 2 tests of Gaussianity and uncorrelated noise, described in Section 3.5.

4. CONCLUSION

Space-based time-series stellar photometry includes many different contributing factors. These include detector noise, spacecraft, instrument, and telescope induced noise, stellar activity, and eclipses. In modeling eclipses (or planetary transits) it is essential to efficiently remove unwanted activity from these time-series datasets both accurately and precisely and without introducing additional non-physical subtle features

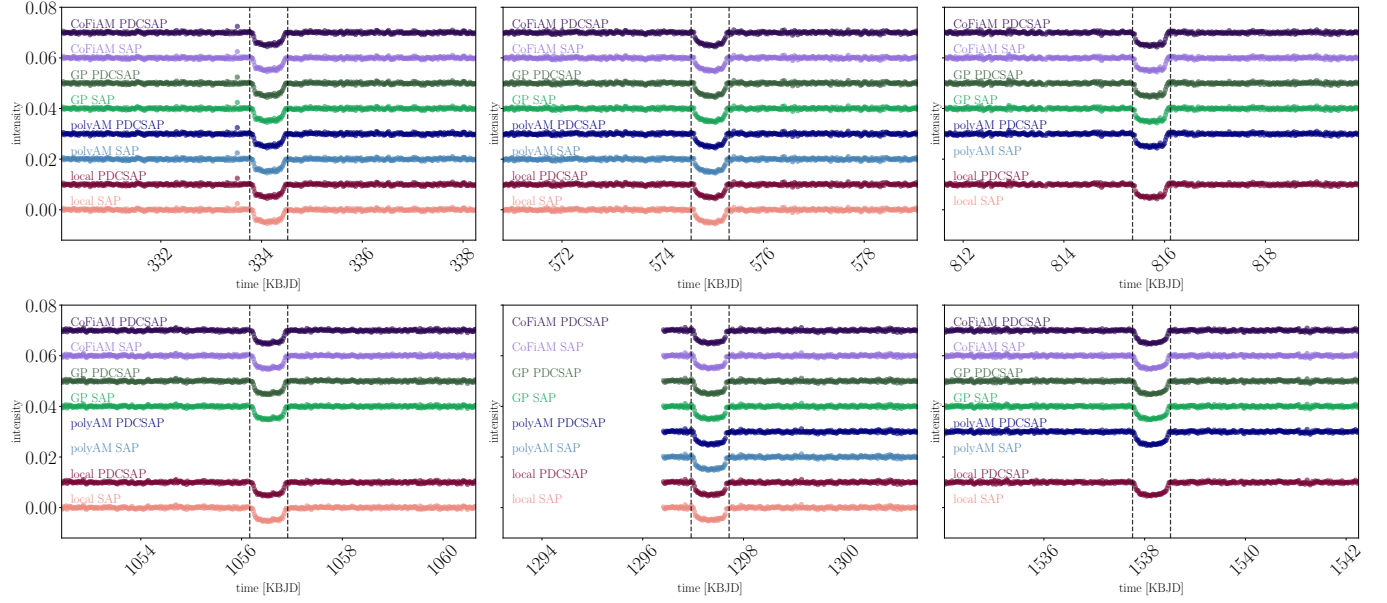


Figure 9. Individually detrended light curves for Kepler-1519 b that passed both tests of correlation. Included in this figure are all 8 default detrending methods in the **democratic detrender**, which are CoFIAM, GP, polyAM, local run on both the SAP data and PDCSAP data. We can see that for the 1st epoch all 8 detrending models passed both tests while for the other 5 epochs, some of the detrending models didn’t pass the both tests. The vertical dashed lines show the in-transit portion of the light curve (LC) that was “masked” and thus not included in the model fitting process. Instead for these portions of the LC, the model fit is extrapolated from the rest of the out-of-transit data such that physical transit features are not removed unintentionally.

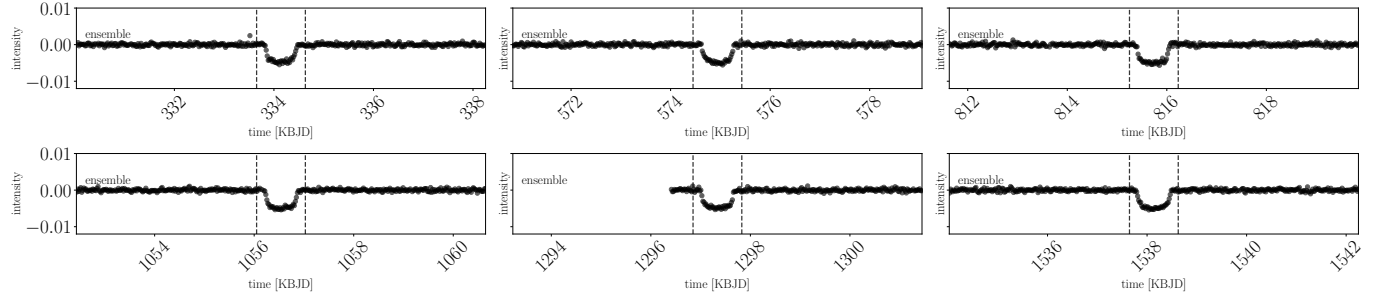


Figure 10. Final ensemble detrended light curves for Kepler-1519 b. Included in this ensemble detrending are all 8 default detrending methods that passed both bootstrapping tests of correlated noise in the **democratic detrender**, which are CoFIAM, GP, polyAM, local run on both the SAP data and PDCSAP data. See Figure 9 for which detrending models passed the tests for each epoch. The vertical dashed lines show the in-transit portion of the light curve (LC) that was “masked” and thus not included in the model fitting process. Instead for these portions of the LC, the model fit is extrapolated from the rest of the out-of-transit data such that physical transit features are not removed unintentionally.

in the data. There exists no perfect model for this unwanted activity, and the many different detrending models used by the exoplanet community each have their own strengths and weaknesses (Hippke et al. 2019).

For modeling transits, space-based time-series will frequently have a baseline of out-of-transit data that greatly exceeds the in-transit data baseline. When this is the case, it is an appropriate approximation to model the transit in a two-stepped approach, first removing unwanted activity and then fitting an exoplanet transit to the detrended data.

When modeling such data where implementing this two-stepped approach is appropriate, in this manuscript we present a new way to mitigate the imperfections of detrending models by detrending via an ensemble-based approach with a community-of-models. We additionally present a set of tests of each individually detrended light curves for correlated noise, ensuring that any detrending model used in the final ensemble detrended light curve is consistent with the expected Gaussian uncorrelated white noise properties.

By doing so, we can reduce the dependency of our final ensemble detrended light curve on the assumptions

of different detrending models – therefore improving our detrended light curve by mitigating model dependency and propagating information regarding uncertainties between the individual detrending models. This can aid in more precise transit modeling and will reduce the likelihood of erroneous non-physical features being propagated into our fitted planetary parameters.

Finally, we present an open-source, modular, and scalable coding package, the `democratic detrender`, that can perform out-of-the-box ensemble detrending on all *Kepler*, *TESS*, and any user-supplied time-series light curve.

D.A.Y. and D.K. acknowledge support from NASA Grant #80NSSC21K0960.

D.A.Y. acknowledges support from the NASA/NY Space Grant

D.A.Y. thanks the LSST-DA Data Science Fellowship Program, which is funded by LSST-DA, the Brinson Foundation, and the Moore Foundation; his participation in the program has benefited this work.

Some of the code used in the `democratic detrender` was adopted from the `MoonPy` package (Teachey & Kipping 2021).

This research made use of `exoplanet` (Foreman-Mackey et al. 2021; Foreman-Mackey et al. 2021) and its dependencies (Kumar et al. 2019; Astropy Collaboration et al. 2013, 2018; Kipping 2013; Salvatier et al. 2016a; Theano Development Team 2016).

This work was supported by patrons to the Cool Worlds Lab, for which the authors thank D. Smith, M. Sloan, C. Bottaccini, D. Daughaday, A. Jones, S. Brownlee, N. Kildal, Z. Star, E. West, T. Zajonc, C. Wolfred, L. Skov, G. Benson, A. De Vaal, M. Elliott, B. Daniluk, M. Forbes, S. Vystoropskyi, S. Lee, Z. Danielson, C. Fitzgerald, C. Souter, M. Gillette, T. Jeffcoat, J. Rockett, D. Murphree, S. Hannum, T. Donkin, K. Myers, A. Schoen, K. Dabrowski, J. Black, R. Ramezankhani, J. Armstrong, K. Weber, S. Marks, L. Robinson, S. Roulier, B. Smith, G. Canterbury, J. Cassese, J. Kruger, S. Way, P. Finch, S. Applegate, L. Watson, E. Zahnle, N. Gebben, J. Bergman, E. Dessoi, J. Alexander, C. Macdonald, M. Hedlund, P. Kaup, C. Hays, W. Evans, D. Bansal, J. Curtin, J. Sturm, RAND Corp., M. Donovan, N. Corwin, M. Mangione, K. Howard, L. Deacon, G. Metts, G. Genova, R. Provost, B. Sigurjonsson, G. Fullwood, B. Walford, J. Boyd, N. De Haan, J. Gillmer, R. Williams, E. Garland, A. Leishman, A. Phan Le, R. Lovely, M. Spoto, A. Steele, M. Varenka, K. Yarbrough, A. Cornejo, D. Compos, F. Demopoulos, G. Bylinsky, J. Werner, B. Pearson, S. Thayer, T. Edris & M. Waters.

Software: `exoplanet` (Foreman-Mackey et al. 2021), `matplotlib` (Hunter 2007), `numpy` (Walt et al. 2011), `scipy` (Jones et al. 2001) `PyMC3` (Salvatier et al. 2016b) `corner` (Foreman-Mackey 2016).

REFERENCES

- Aigrain, S., Parviainen, H., & Pope, B. J. S. 2016, *MNRAS*, 459, 2408, doi: [10.1093/mnras/stw706](https://doi.org/10.1093/mnras/stw706)
- Angus, R., Morton, T., Aigrain, S., Foreman-Mackey, D., & Rajpaul, V. 2017, *Monthly Notices of the Royal Astronomical Society*, 474, 2094, doi: [10.1093/mnras/stx2109](https://doi.org/10.1093/mnras/stx2109)
- Astropy Collaboration, Robitaille, T. P., Tollerud, E. J., et al. 2013, *aap*, 558, A33, doi: [10.1051/0004-6361/201322068](https://doi.org/10.1051/0004-6361/201322068)
- Astropy Collaboration, Price-Whelan, A. M., Sip Hocz, B. M., et al. 2018, *aj*, 156, 123, doi: [10.3847/1538-3881/aabc4f](https://doi.org/10.3847/1538-3881/aabc4f)
- Auvergne, M., Bodin, P., Boisdard, L., et al. 2009, *A&A*, 506, 411, doi: [10.1051/0004-6361/200810860](https://doi.org/10.1051/0004-6361/200810860)
- Bakos, G., Noyes, R. W., Kovács, G., et al. 2004, *PASP*, 116, 266, doi: [10.1086/382735](https://doi.org/10.1086/382735)
- Benz, W., Broeg, C., Fortier, A., et al. 2021, *Experimental Astronomy*, 51, 109, doi: [10.1007/s10686-020-09679-4](https://doi.org/10.1007/s10686-020-09679-4)
- Borucki, W. J., Koch, D., Basri, G., et al. 2010, *Science*, 327, 977, doi: [10.1126/science.1185402](https://doi.org/10.1126/science.1185402)
- Carter, J. A., & Winn, J. N. 2009, *ApJ*, 704, 51, doi: [10.1088/0004-637X/704/1/51](https://doi.org/10.1088/0004-637X/704/1/51)
- Dasarathy, B., & Sheela, B. 1979, *Proceedings of the IEEE*, 67, 708, doi: [10.1109/PROC.1979.11321](https://doi.org/10.1109/PROC.1979.11321)
- Durbin, J., & Watson, G. S. 1950, *Biometrika*, 37, 409, doi: [10.1093/biomet/37.3-4.409](https://doi.org/10.1093/biomet/37.3-4.409)
- Fabrycky, D. C., Ford, E. B., Steffen, J. H., et al. 2012, *ApJ*, 750, 114, doi: [10.1088/0004-637X/750/2/114](https://doi.org/10.1088/0004-637X/750/2/114)
- Foreman-Mackey, D. 2016, *The Journal of Open Source Software*, 1, 24, doi: [10.21105/joss.00024](https://doi.org/10.21105/joss.00024)
- . 2018, *Research Notes of the American Astronomical Society*, 2, 31, doi: [10.3847/2515-5172/aaaf6c](https://doi.org/10.3847/2515-5172/aaaf6c)
- Foreman-Mackey, D., Agol, E., Ambikasaran, S., & Angus, R. 2017, *AJ*, 154, 220, doi: [10.3847/1538-3881/aa9332](https://doi.org/10.3847/1538-3881/aa9332)
- Foreman-Mackey, D., Savel, A., Luger, R., et al. 2021, *exoplanet-dev/exoplanet v0.4.5*, doi: [10.5281/zenodo.1998447](https://doi.org/10.5281/zenodo.1998447)
- Foreman-Mackey, D., Luger, R., Agol, E., et al. 2021, *arXiv e-prints*, arXiv:2105.01994, <https://arxiv.org/abs/2105.01994>
- Foreman-Mackey, D., Savel, A., Luger, R., et al. 2021, *exoplanet-dev/exoplanet v0.5.1*, doi: [10.5281/zenodo.1998447](https://doi.org/10.5281/zenodo.1998447)
- Gaia Collaboration, Prusti, T., de Bruijne, J. H. J., et al. 2016, *A&A*, 595, A1, doi: [10.1051/0004-6361/201629272](https://doi.org/10.1051/0004-6361/201629272)
- Gautier, Thomas N., I., Charbonneau, D., Rowe, J. F., et al. 2012, *ApJ*, 749, 15, doi: [10.1088/0004-637X/749/1/15](https://doi.org/10.1088/0004-637X/749/1/15)
- Ge, J., Zhang, H., Zang, W., et al. 2022, *arXiv e-prints*, arXiv:2206.06693, doi: [10.48550/arXiv.2206.06693](https://doi.org/10.48550/arXiv.2206.06693)
- Giles, H. A. C., Bayliss, D., Espinoza, N., et al. 2018, *MNRAS*, 475, 1809, doi: [10.1093/mnras/stx3300](https://doi.org/10.1093/mnras/stx3300)
- Gilliland, R. L., Chaplin, W. J., Jenkins, J. M., Ramsey, L. W., & Smith, J. C. 2015, *AJ*, 150, 133, doi: [10.1088/0004-6256/150/4/133](https://doi.org/10.1088/0004-6256/150/4/133)
- Gilliland, R. L., Jenkins, J. M., Borucki, W. J., et al. 2010, *ApJL*, 713, L160, doi: [10.1088/2041-8205/713/2/L160](https://doi.org/10.1088/2041-8205/713/2/L160)
- Gilliland, R. L., Chaplin, W. J., Dunham, E. W., et al. 2011, *ApJS*, 197, 6, doi: [10.1088/0067-0049/197/1/6](https://doi.org/10.1088/0067-0049/197/1/6)
- Hansen, L., & Salamon, P. 1990, *IEEE Transactions on Pattern Analysis and Machine Intelligence*, 12, 993, doi: [10.1109/34.58871](https://doi.org/10.1109/34.58871)
- Hattori, S., Foreman-Mackey, D., Hogg, D. W., et al. 2022, *AJ*, 163, 284, doi: [10.3847/1538-3881/ac625a](https://doi.org/10.3847/1538-3881/ac625a)
- Hippke, M., David, T. J., Mulders, G. D., & Heller, R. 2019, *AJ*, 158, 143, doi: [10.3847/1538-3881/ab3984](https://doi.org/10.3847/1538-3881/ab3984)
- Howell, S. B., Sobek, C., Haas, M., et al. 2014, *PASP*, 126, 398, doi: [10.1086/676406](https://doi.org/10.1086/676406)
- Hunter, J. D. 2007, *Computing in Science and Engineering*, 9, 90, doi: [10.1109/MCSE.2007.55](https://doi.org/10.1109/MCSE.2007.55)
- Ivezić, Ž., Kahn, S. M., Tyson, J. A., et al. 2019, *ApJ*, 873, 111, doi: [10.3847/1538-4357/ab042c](https://doi.org/10.3847/1538-4357/ab042c)
- Jenkins, J. M., Caldwell, D. A., Chandrasekaran, H., et al. 2010, *ApJL*, 713, L120, doi: [10.1088/2041-8205/713/2/L120](https://doi.org/10.1088/2041-8205/713/2/L120)
- Jones, E., Oliphant, T., Peterson, P., et al. 2001, *SciPy: Open source scientific tools for Python*, <http://www.scipy.org/>
- Kim, D.-W., Protopapas, P., Alcock, C., Byun, Y.-I., & Bianco, F. B. 2009, *MNRAS*, 397, 558, doi: [10.1111/j.1365-2966.2009.14967.x](https://doi.org/10.1111/j.1365-2966.2009.14967.x)
- Kipping, D., Solano-Oropeza, D., Yahalomi, D., et al. 2024, submitted, *M/K-Dwarf Exoplanets With Similar Sizes and Instellations to Earth Typically Follow Near-Circular Orbits*
- Kipping, D., & Yahalomi, D. A. 2023, *MNRAS*, 518, 3482, doi: [10.1093/mnras/stac3360](https://doi.org/10.1093/mnras/stac3360)
- Kipping, D., Bryson, S., Burke, C., et al. 2022, *Nature Astronomy*, 6, 367, doi: [10.1038/s41550-021-01539-1](https://doi.org/10.1038/s41550-021-01539-1)
- Kipping, D. M. 2013, *mnras*, 434, L51, doi: [10.1093/mnrasl/slt075](https://doi.org/10.1093/mnrasl/slt075)
- Kipping, D. M., Hartman, J., Buchhave, L. A., et al. 2013, *ApJ*, 770, 101, doi: [10.1088/0004-637X/770/2/101](https://doi.org/10.1088/0004-637X/770/2/101)
- Kipping, D. M., & Tinetti, G. 2010, *MNRAS*, 407, 2589, doi: [10.1111/j.1365-2966.2010.17094.x](https://doi.org/10.1111/j.1365-2966.2010.17094.x)

- Kumar, R., Carroll, C., Hartikainen, A., & Martin, O. A. 2019, *The Journal of Open Source Software*, doi: [10.21105/joss.01143](https://doi.org/10.21105/joss.01143)
- Lightkurve Collaboration, Cardoso, J. V. d. M., Hedges, C., et al. 2018, *Lightkurve: Kepler and TESS time series analysis in Python*, *Astrophysics Source Code Library*. <http://ascl.net/1812.013>
- Luger, R., Agol, E., Kruse, E., et al. 2016, *AJ*, 152, 100, doi: [10.3847/0004-6256/152/4/100](https://doi.org/10.3847/0004-6256/152/4/100)
- Luger, R., Kruse, E., Foreman-Mackey, D., Agol, E., & Saunders, N. 2018, *AJ*, 156, 99, doi: [10.3847/1538-3881/aad230](https://doi.org/10.3847/1538-3881/aad230)
- Mazeh, T., & Faigler, S. 2010, *A&A*, 521, L59, doi: [10.1051/0004-6361/201015550](https://doi.org/10.1051/0004-6361/201015550)
- Mazeh, T., Tamuz, O., & Zucker, S. 2007, in *Astronomical Society of the Pacific Conference Series*, Vol. 366, *Transiting Extrapolar Planets Workshop*, ed. C. Afonso, D. Weldrake, & T. Henning, 119, doi: [10.48550/arXiv.astro-ph/0612418](https://doi.org/10.48550/arXiv.astro-ph/0612418)
- McGruder, C. D., López-Morales, M., Kirk, J., et al. 2022, *AJ*, 164, 134, doi: [10.3847/1538-3881/ac7f2e](https://doi.org/10.3847/1538-3881/ac7f2e)
- Morvan, M., Nikolaou, N., Tsiaras, A., & Waldmann, I. P. 2020, *AJ*, 159, 109, doi: [10.3847/1538-3881/ab6aa7](https://doi.org/10.3847/1538-3881/ab6aa7)
- Ofir, A., Alonso, R., Bonomo, A. S., et al. 2010, *MNRAS*, 404, L99, doi: [10.1111/j.1745-3933.2010.00843.x](https://doi.org/10.1111/j.1745-3933.2010.00843.x)
- Pepper, J., Pogge, R. W., DePoy, D. L., et al. 2007, *PASP*, 119, 923, doi: [10.1086/521836](https://doi.org/10.1086/521836)
- Pollacco, D. L., Skillen, I., Collier Cameron, A., et al. 2006, *PASP*, 118, 1407, doi: [10.1086/508556](https://doi.org/10.1086/508556)
- Pont, F., Zucker, S., & Queloz, D. 2006, *MNRAS*, 373, 231, doi: [10.1111/j.1365-2966.2006.11012.x](https://doi.org/10.1111/j.1365-2966.2006.11012.x)
- Rauer, H., Catala, C., Aerts, C., et al. 2014, *Experimental Astronomy*, 38, 249, doi: [10.1007/s10686-014-9383-4](https://doi.org/10.1007/s10686-014-9383-4)
- Ricker, G. R., Winn, J. N., Vanderspek, R., et al. 2015, *Journal of Astronomical Telescopes, Instruments, and Systems*, 1, 014003, doi: [10.1117/1.JATIS.1.1.014003](https://doi.org/10.1117/1.JATIS.1.1.014003)
- Salvatier, J., Wiecki, T. V., & Fonnesbeck, C. 2016a, *PeerJ Computer Science*, 2, e55
- . 2016b, *PeerJ Computer Science*, 2, e55
- Sandford, E., & Kipping, D. 2017, *AJ*, 154, 228, doi: [10.3847/1538-3881/aa94bf](https://doi.org/10.3847/1538-3881/aa94bf)
- Schapire, R. 1990, *Machine Learning*, 5, 197, doi: [10.1023/A:1022648800760](https://doi.org/10.1023/A:1022648800760)
- Schwarz, G. 1978, *The Annals of Statistics*, 6, 461. <http://www.jstor.org/stable/2958889>
- Smith, J. C., Stumpe, M. C., Van Cleve, J. E., et al. 2012, *PASP*, 124, 1000, doi: [10.1086/667697](https://doi.org/10.1086/667697)
- Spergel, D., Gehrels, N., Baltay, C., et al. 2015, *arXiv e-prints*, arXiv:1503.03757. <https://arxiv.org/abs/1503.03757>
- Stumpe, M. C., Smith, J. C., Van Cleve, J. E., et al. 2012, *PASP*, 124, 985, doi: [10.1086/667698](https://doi.org/10.1086/667698)
- Teachey, A., & Kipping, D. 2021, *MNRAS*, 508, 2620, doi: [10.1093/mnras/stab2694](https://doi.org/10.1093/mnras/stab2694)
- Teachey, A., & Kipping, D. M. 2018, *Science Advances*, 4, eaav1784, doi: [10.1126/sciadv.aav1784](https://doi.org/10.1126/sciadv.aav1784)
- Theano Development Team. 2016, *arXiv e-prints*, abs/1605.02688. <http://arxiv.org/abs/1605.02688>
- Vanderburg, A., & Johnson, J. A. 2014, *PASP*, 126, 948, doi: [10.1086/678764](https://doi.org/10.1086/678764)
- Waldmann, I. P. 2014, *ApJ*, 780, 23, doi: [10.1088/0004-637X/780/1/23](https://doi.org/10.1088/0004-637X/780/1/23)
- Waldmann, I. P., Tinetti, G., Drossart, P., et al. 2012, *ApJ*, 744, 35, doi: [10.1088/0004-637X/744/1/35](https://doi.org/10.1088/0004-637X/744/1/35)
- Walt, S. v. d., Colbert, S. C., & Varoquaux, G. 2011, *Computing in Science and Eng.*, 13, 22, doi: [10.1109/MCSE.2011.37](https://doi.org/10.1109/MCSE.2011.37)
- Yahalomi, D. A., Kipping, D., Nesvorný, D., et al. 2024, *MNRAS*, 527, 620, doi: [10.1093/mnras/stad3070](https://doi.org/10.1093/mnras/stad3070)
- Zhang, C., & Ma, Y. 2012, *Ensemble machine learning: Methods and applications*, 1–329, doi: [10.1007/9781441993267](https://doi.org/10.1007/9781441993267)